Optical Engineering

SPIEDigitalLibrary.org/oe

Automatic identification and removal of outliers for high-speed fringe projection profilometry

Shijie Feng
Qian Chen
Chao Zuo
Rubin Li
Guochen Shen
Fangxiaoyu Feng

Automatic identification and removal of outliers for high-speed fringe projection profilometry

Shijie Feng
Qian Chen
Nanjing University of Science and Technology
Jiangsu Key Laboratory of Spectral Imaging & Intelligence Sense
Nanjing, Jiangsu Province 210094, China
and
Ministry of Education of China
Beijing Institute of Technology
Key Laboratory of Photoelectronic Imaging Technology and System
Beijing 100081, China
E-mail: geniusshijie@163.com

Chao Zuo
Rubin Li
Guochen Shen
Fangxiaoyu Feng
Nanjing University of Science and Technology
Jiangsu Key Laboratory of Spectral Imaging & Intelligence Sense
Nanjing, Jiangsu Province 210094, China

Abstract. Phase-shifting profilometry combining with the two-frequency temporal phase unwrapping is widely used for high-speed, real-time acquisition of three-dimensional shapes. However, when the object is not motionless during the acquisition process, some unreliable results may emerge, especially around the contours of the measured object. The main reason for this is that the same point in the projected pattern sequence can map to different points within the camera images resulting from depth changes over time. We present a novel approach for identifying those invalid pixels affected by such an error. By carefully examining the captured fringe pattern, comparing two modulation maps, utilizing the phase relationship between two neighboring pixels, and employing a Gaussian filter to detect the protruding points, the bad measurement pixels can be detected and filtered out effectively. The whole procedure is of low computational complexity because of the introduced lookup table-based fast data processing method. Some experimental results are presented to verify the validity of our method. © *2013 Society of Photo-Optical Instrumentation Engineers (SPIE).* [DOI: 10.1117/1.OE.52.1.013605]

Subject terms: invalid pixel identification; high-speed fringe projection; three-dimensional measurement; moving object.

Paper 121179 received Aug. 14, 2012; revised manuscript received Nov. 21, 2012; accepted for publication Dec. 17, 2012; published online Jan. 9, 2013.

1 Introduction

A structured light measurement system based on a simple triangulation technique has been widely adopted in optical, noncontact, three-dimensional metrology over the years.[1,2] With recent progress in digital projection devices, generating and manipulating the fringe patterns with an off-the-shelf digital light processing (DLP) projector has become feasible. The high-speed, real-time, three-dimensional (3-D) shape measurement relied on digital fringe projection has vast potentials for future development in many fields, including modern industry inspection, rapid reverse engineering, biomedical sciences and entertainment, attribute to its properties of high resolution, time-saving and low costs.[3]

In high-speed, real-time measurement systems, however, there are still several problems that facing researchers. First, despite the short acquisition period, when the scanned object is not motionless, it violates the basic phase-shift assumption that corresponding pixels in the phase images depict the same surface point, resulting in a large number of unreliable pixels at the object edges.[4–6] Second, the measurement results are especially susceptible to error introduced from camera/projector noise and the instable ambient light.[7,8] Generally, a 3-D reconstruction result of reliability and accuracy is achieved with high rates of projection and capture.[9–11] But as the rates are increasing, a camera lacking sufficient exposure time coupled with the increasing effect of ambient light will unexpectedly lead to noises either from the system itself or outside surroundings, which will produce invalid damaging points to the measurement result. In order to cope with the problems above, Zhang[12] proposed a solution of reducing error points by using phase monotonicity. Chen et al.[13] presented a new method in identifying the abrupt discontinuities on the object surface. And Huang et al.[14] combined Zhang's and Chen et al.'s methods before providing an invalid phase identification framework based on temporal phase unwrapping method. But these methods are designed for static scene measurement in which at least three phase maps are acquired to generate an accurate phase map with high resolution. Obviously, for some dynamic applications, those methods are no longer applicable because the two-frequency phase unwrapping method is commonly employed to minimize the acquisition time. Lau et al.[5] proposed a method used in detection of edge errors for a moving object, which is based on a traditional phase-shifting algorithm and the discrete Fourier transform. However, a comprehensive framework for incorrect pixel identification in high-speed phase-shifting profilometry coupled with the two-frequency temporal phase unwrapping is still lacking.

In this paper, we present a novel and systematic four-step approach to eliminate invalid pixels in the procedure of 3-D reconstruction of moving object, which employs phase maps, captured fringe patterns, modulation maps derived of two-frequency temporal phase-unwrapping algorithms, and a Gaussian filter to detect unreliable pixels. Considering the traditional data processing method may not meet the requirement of fast data computation, an introduced lookup table (LUT)-based fast data processing algorithm is used to lower the computational complexity and reduce the time cost of our work. The experimental results indicate the proposed approach is reliable and robust.

2 Principle

In Sec. 2.1, we first briefly review the phase-shifting algorithm and two-frequency phase-unwrapping method, which

are the most widely employed techniques in high-speed, real-time shape measurement. Then, we detail our invalid pixels identification algorithm and LUT-based fast data processing method in Secs. 2.2–2.6.

2.1 *Phase-Shifting Algorithm and Two-Frequency Phase-Unwrapping Method*

A typical phase-shifting profilometry system is given in Fig. 1. The fringe patterns consisting of vertical or horizontal sinusoidal stripes are sent to a projector. Then they are projected by the projector and modulated by the surface of measured object. By utilizing a camera, the distorted stripes can be captured and sent to a computer for data analysis and processing.

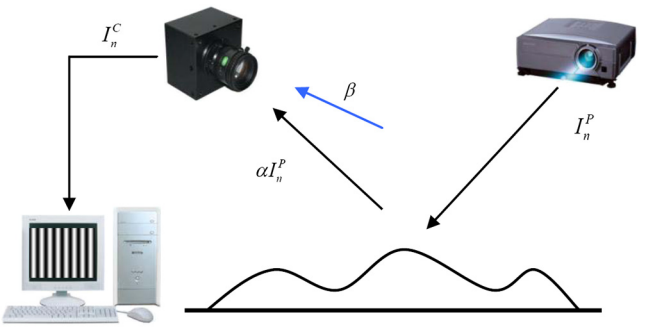

Fig. 1 A typical phase-shifting profilometry system.

2.1.1 *Fringe projection*

N-step phase-shifting algorithms, such as a three-step or four-step phase-shifting algorithm, are extensively used to obtain phase values. The intensities of the patterns to be projected can be written as follows:

$$I_n^P(x^P, y^P) = A^P(x^P, y^P) + B^P(x^P, y^P)\cos[\phi^P(x^P, y^P) + 2\pi n/N], \quad (1)$$

where (x^P, y^P) is the pixel coordinate in the projector, $A^P(x^P, y^P)$ is the temporal DC value, and $B^P(x^P, y^P)$ is the amplitude of the temporal AC value. Generally, these patterns are generated by computer, so we have $A^P(x^P, y^P) = B^P(x^P, y^P)$; n is the phase-shift index, and N is the total number of phase shifts.

2.1.2 *Fringe acquisition*

We assume that (x, y) is the pixel coordinate in the camera and $\alpha(x, y)$ is the reflectivity of a measured object captured by pixel (x, y). After the projected fringe patterns have been reflected by a measured object, and with the consideration of the impact of the ambient light intensity $\beta(x, y)$ in the measuring scene, the intensities of the patterns captured by camera can be

$$I_n^C(x, y) = \alpha(x, y)\{A^P(x, y) + B^P(x, y)\cos[\phi(x, y) + 2\pi n/N]\} + \beta(x, y). \quad (2)$$

After simplification, we have

$$I_n^C(x, y) = A^C(x, y) + B^C(x, y)\cos[\phi(x, y) + 2\pi n/N], \quad (3)$$

where $A^C(x, y)$ is the average intensity, which equals to $\alpha(x, y)A^P(x, y) + \beta(x, y)$, and $B^C(x, y)$ is the intensity modulation, which equals to $\alpha(x, y)B^P(x, y)$, $\phi(x, y)$ is the phase to be solved.

2.1.3 *Phase retrieval*

The $\phi(x, y)$ above can be retrieved by the following Eq. (4), and the average intensity and intensity modulation can be solved by the next two equations separately.

$$\phi(x, y) = \tan^{-1}\frac{\sum_{n=1}^{N} I_n^C(x, y)\sin(2\pi n/N)}{\sum_{n=1}^{N} I_n^C(x, y)\cos(2\pi n/N)}. \quad (4)$$

$$A^C(x, y) = \frac{\sum_{n=1}^{N} I_n^C(x, y)}{N}. \quad (5)$$

$$B^C(x, y) = \frac{2}{N}\sqrt{\left[\sum_{n=1}^{N} I_n^C(x, y)\sin(2\pi n/N)\right]^2 + \left[\sum_{n=1}^{N} I_n^C(x, y)\cos(2\pi n/N)\right]^2}. \quad (6)$$

The value of $\phi(x, y)$, solved from Eq. (4), ranges from $-\pi$ to $+\pi$. If the projected patterns contain only one sinusoidal fringe, then the phase value $\phi(x, y)$ is not required to be unwrapped. However, its accuracy is not adequate to be used in many 3-D reconstructions. Thus, projected patterns with multiple sinusoidal fringes are usually adopted to achieve a more precise phase map. But its phase value contains 2π discontinuities, which need to be removed by a phase-unwrapping algorithm. Phase-unwrapping algorithms consist of spatial phase-unwrapping algorithms and temporal phase-unwrapping algorithms. Spatial phase-unwrapping algorithms cannot resolve the phase ambiguity in discontinuous surfaces and large step-height changes where the phase changes large than π. Therefore, temporal phase-unwrapping algorithms are usually employed to retrieve phase value. To reduce the number of projected patterns, two-frequency temporal phase-unwrapping algorithms are widely used in real-time, high-speed measurements, which can be described as follows:

$$\Phi(x, y) = \phi(x, y) + 2\pi N \quad (7)$$

$$N = Round\left[\frac{k\phi'(x, y) - \phi(x, y)}{2\pi}\right], \quad (8)$$

where $\Phi(x,y)$ is the unwrapped phase, ϕ' is the low-frequency phase, and ϕ the high-frequency phase, $Round(\bullet)$ is to get the nearest integer; k satisfies the relationship $f_H = kf_L$, where f_L is the frequency of ϕ' and f_H the frequency of ϕ. Particularly, suppose the projector has a resolution of $W \times H$ and the projected fringe patterns are vertical, the low-frequency means the wavelength $\lambda_L = W$.[7,12] In this way, a phase map derived from low frequency patterns is directly acquired without any phase-unwrapping method, and then it is applied to extract wrapped phase map from high frequency patterns with the purpose of obtaining a phase map with high resolution.

2.1.4 *Depth information acquisition*

The schematic diagram is shown in Fig. 2. A reference plane is measured first and the depth of object $H(x,y)$ is measured relative to this plane. From the view of projector, the points A and B have the same phase value. Meanwhile, from the view of camera, points B and C are captured by the same pixel. Considering the phase of reference plane, we have the phase difference of this specific pixel,

$$\Phi_{\mathrm{BC}} = \Phi_{\mathrm{AC}} = \Phi_A - \Phi_C. \tag{9}$$

Apparently, $\triangle ABC$ and $\triangle EBD$ are similar, therefore we have

$$\frac{l}{\overline{\mathrm{AC}}} = \frac{d - H(x,y)}{H(x,y)} = \frac{d}{H(x,y)} - 1. \tag{10}$$

This equation can be simplified as follows:[15]

$$H(x,y) = \frac{d\overline{\mathrm{AC}}}{\overline{\mathrm{AC}} + l} = \frac{d\Phi_{\mathrm{AC}}}{\Phi_{\mathrm{AC}} + 2\pi lf}, \tag{11}$$

where Φ_{AC} is phase difference between points A and C, d is the distance from reference plane to the entrance pupil of the camera, l is the distance between the exit pupil of the projector and entrance pupil of the camera, and f the frequency of projected fringe pattern.

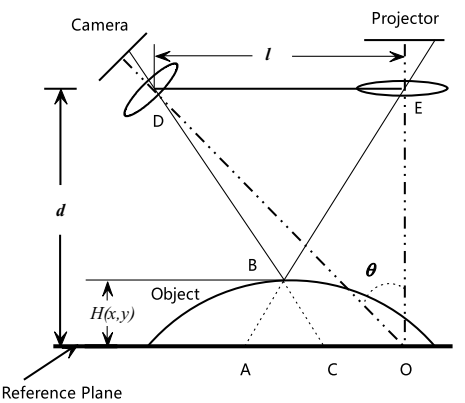

Fig. 2 Schematic diagram of phase-to-depth conversion.

2.2 *Phase Invalid Pixels Detection: Utilizing Phase Value and Captured Intensities of the Tested Pixel*

Commonly, the pixels with unreliable phase values are treated as the so-called invalid pixels. For a moving object, we have to face a fact that in one period of phase shift, some of the fringe patterns reflected by a specific point on a measured object will be captured and displayed by a pixel on a charge coupled device (CCD) array, but because of the motion of the object, other point with different material on the object may reflect the rest fringe patterns which it shall not reflect and consequently, the captured intensities at that pixel may be abnormal. Using those unreliable intensities to solve Eq. (4) is the major reason for an incorrect phase value. For further analysis, a pixel on CCD array corresponds with a point on measured object. The CCD pixel can capture the intensity of fringe patterns distorted by the object because of the reflection occurring at the object. However, if some of the fringe patterns fail to be projected to that point on the measured object due to the object's movement, it may result in no reflected light being captured by that corresponding CCD pixel. In brief, in one period of phase shift, if the reflectivity captured by the same pixel changes drastically, we can identify that pixel as an invalid pixel. Furthermore, because of the strong variation of reflectivity at that pixel, its calculated phase value will be incorrect. Hence, in order to detect invalid pixel, two directions can be taken into account. One is to detect the correctness of the phase value at each CCD pixel, and the other is to judge the variation of reflectivity at the pixel. In this subsection, we provide a method which relies on the first direction to detect "bad" pixels.

The principle of the method can be described as follows. First, a phase-shifting method is used to recover the phase value at each pixel. Then let us suppose that these phase values are all correct. To test the validity of the hypothesis, we need to find another way to compute a new phase value at the same pixel. If the two phase values are close enough, the hypothesis stands and the tested pixel is a valid one. Otherwise, the hypothesis is incorrect and the tested pixel is invalid. To achieve a new phase value from a different way, Eq. (3) can be used since I_n^C is the captured intensity by the camera, A^C and B^C can be calculated by Eqs. (5) and (6). So we have

$$\cos[\Phi'(x,y) + 2\pi n/N] = \frac{I_n^C - A^C(x,y)}{B^C(x,y)}, \tag{12}$$

where $\Phi'(x,y)$ is the new phase value. However, solving the $\Phi'(x,y)$ from $\cos(\bullet)$ is an inconvenient and time-consuming job which is inappropriate for high-speed, real-time measurement. To tackle this problem, our solution is remaining $\Phi'(x,y)$ in the form of $\cos(\bullet)$, which is described as follows:

$$K_n' = \cos[\Phi'(x,y) + 2\pi n/N] = \frac{I_n^C - A^C(x,y)}{B^C(x,y)}. \tag{13}$$

Meanwhile we put the phase value derived from the phase-shifting algorithm into the form of $\cos(\bullet)$, and we have

$$K_n'' = \cos[\Phi(x,y) + 2\pi n/N]. \tag{14}$$

Comparing the two phase values is replaced by comparing K'_n and K''_n. When the N-step phase-shifting is adopted, we have N pairs of K'_n and K''_n for each pixel. The root mean square error (*Error*) is used to quantify the difference between the two groups of phase values.

$$Error = \sqrt{\frac{\sum_{n=1}^{N}(K'_n - K''_n)^2}{N}}, \tag{15}$$

where N is the total number of phase shifts. By setting a threshold to *Error*, those incorrect pixels can be identified and then eliminated in the subsequent processing.

For a better understanding of this method, here we present an instance, in which we use six-step phase-shifting algorithm to illustrate it. The received intensities by a valid pixel are $I_n^C(x,y)$ $(n = 1,2,3,4,5,6)$. Obviously, they will be seated at an ideal sinusoidal wave, as shown in Fig. 3(a). By employing Eqs. (4)–(6), coupled with unwrapping method, phase value, average intensity, and modulation are obtained. After solving Eqs. (13) and (14), K'_n and K''_n are acquired and described by red dots, as shown in Fig. 3(b). We will find that K'_n and K''_n coincide. It turns out that the pixel is a "good" pixel. However, if the tested pixel is an unreliable pixel, its captured intensities $I_n^C(x,y)$ will not distribute on an ideal sinusoidal waveform, as shown in Fig. 3(c). Its K'_n and K''_n values are shown in Fig. 3(d), in which K''_n, represented by the red triangles, does not match K'_n, indicated by red dots (color online). By the way of calculating root mean square error (*Error*) and setting a threshold to it, the "bad" pixels are detected.

2.3 *Phase Invalid Pixels Detection: Comparing Modulations of Each Pixel*

In this subsection, we start unreliable point detection with the way of testing the captured reflectivity of each pixel. However, it is complicated because the reflectivity cannot be reliably obtained in a phase-shifting method. Fortunately, there exists a useful relationship between reflectivity and intensity modulation. We can use the method of detecting modulation to simplify the process of detecting reflectivity. In principle, for the same material the reflectivity will not change, and as we discussed above, the modulation of the corresponding pixel equals its reflectivity times a constant (B^P), therefore the modulation of tested pixel is invariant too. As a two-frequency phase-unwrapping algorithm is adopted, for each pixel, we have two modulations; one is derived from the high frequency patterns and the other from the low frequency patterns. So, we can compare the values of these two modulations. For a "good" pixel, these two values should be close enough. If they differ greatly, which means the reflectivity varies sharply, then the tested pixel is a "bad" pixel. For some points with low reflectivity, the reflected pattern is nearly invisible and phase noise is significant, so we use relative error of two modulations to judge the reliability of the phase value. We have a criterion as follows:

$$\frac{\mathrm{abs}[B^C_{\mathrm{High}}(x,y) - B^C_{\mathrm{Low}}(x,y)]}{0.5 \times [B^C_{\mathrm{High}}(x,y) + B^C_{\mathrm{Low}}(x,y)]} < \sigma, \tag{16}$$

where $\mathrm{abs}(\bullet)$ is the absolute value. $B^C_{\mathrm{High}}(x,y)$ is the modulation calculated from high frequency fringe images, and

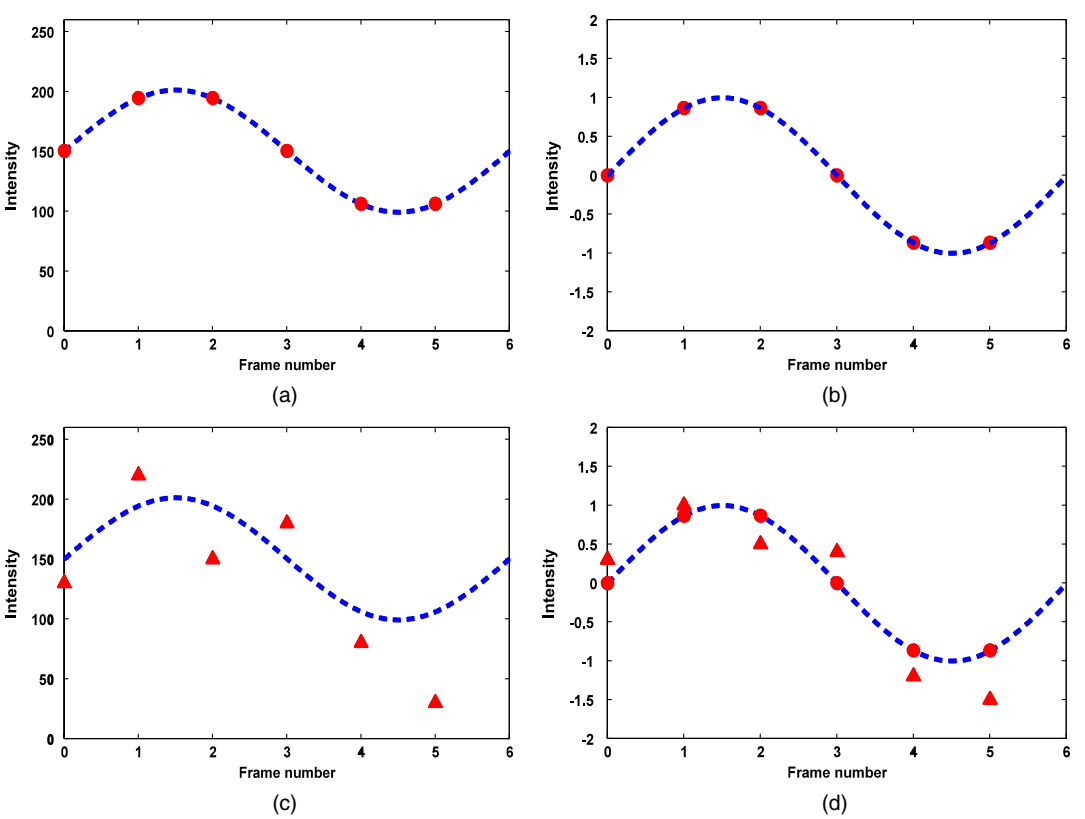

Fig. 3 Comparison between a "good" pixel and "bad" pixel: (a) captured intensities of a "good" pixel during one phase shift period; (b) six pairs of K'_n and K''_n values for a "good" pixel; (c) captured intensities of a "bad" pixel during one phase shift period; (d) six pairs of K'_n and K''_n values for a "bad" pixel.

$B^C_{\mathrm{Low}}(x,y)$ the modulation calculated from low frequency fringe images. By setting a threshold, the pixels that do not satisfy Eq. (16) will be identified.

2.4 *Invalid Pixels Detection by Phase Monotonicity*

From the knowledge of phase-shifting and phase-unwrapping methods, it is evident that the unwrapped phase value increases or decreases along the direction perpendicular to fringe pattern.[12] Assuming the stripes are vertical, theoretically, the correct unwrapped phase should be monotonously increasing or decreasing along the horizontal direction, and we have

$$\Phi(x+1,y) < \Phi(x,y) \quad \text{or} \quad \Phi(x+1,y) > \Phi(x,y). \tag{17}$$

However, in practical application, random noises arising from the measurement system may result in some slightly changed phase values of valid pixels. Therefore, for robustness, Eq. (17) is modified.

$$\begin{aligned} &\Delta_1 < \Phi(x+1,y) - \Phi(x,y) < \Delta_2 \quad \text{or} \\ &\quad \Delta_1 < \Phi(x,y) - \Phi(x+1,y) < \Delta_2. \end{aligned} \tag{18}$$

By properly setting the constraints of the criterion above, the pixels that do not satisfy Eq. (18) are required to be eliminated.

2.5 *Utilizing Smoothed Phase Map to Identify Invalid Pixels*

One of the most prominent characters of invalid pixels is their final phase values are usually much larger/smaller than those of their neighborhoods. Here, the final phase value means the unwrapped phase value after subtracting the phase at the reference plane, namely, the phase difference at the tested pixel. As a consequence, we need to find a method which can tell the protrude values apart. According to acquired knowledge and practical experience, the intensity of a pixel can be replaced by its neighborhoods after being smoothed by a Gaussian filter. Therefore, Gaussian filter possesses the ability of locating the unusual value. So we first use a Gaussian filter to smooth a final phase map, theoretically, the incorrect phase values are averaged by their neighboring phases. Then we match it to the origin final phase map, which has not been filtered by the Gaussian filter. As a result, incorrect phase values will stand out. This criterion is shown as follows:

$$\mathrm{abs}[\tilde{\phi}(x,y) - \tilde{\phi}_G(x,y)] < V, \tag{19}$$

where $\tilde{\phi}_G(x,y)$ is the smoothed final phase map, and $\tilde{\phi}(x,y)$ the origin final phase map. Setting a threshold to V, the pixels do not satisfy the equation above are "bad" pixels.

2.6 *LUT-Based Fast Data Processing*

Since retrieving a value from memory is much faster than experiencing a complicated computation, LUT-based data processing is widely adopted in the situation where minimum processing time is required. In traditional phase-shifting and phase-unwrapping methods, one obtains the phase value and intensity modulation by solving Eqs. (4) and (6), which is time-consuming and not appropriate for real-time measurement. To overcome this problem, an LUT-based algorithm is introduced Ref. 9. Equations (4) and (6) can be simplified according to a specific total number of phase shift N. For $N = 4$,

$$\phi = \tan^{-1}\frac{I^C_1 - I^C_3}{I^C_4 - I^C_2}. \tag{20}$$

$$B^c(x,y) = \frac{1}{2}\sqrt{(I^C_1 - I^C_3)^2 + (I^C_4 - I^C_2)^2}. \tag{21}$$

LUTs for phase value and modulation are defined as follows,

$$\mathrm{LUTPhase}(X,Y) = \tan^{-1}\frac{X}{Y}. \tag{22}$$

$$\mathrm{LUTModulation}(X,Y) = \frac{1}{2}\sqrt{(X)^2 + (Y)^2}. \tag{23}$$

$$X = I^C_1 - I^C_3 \quad \text{and} \quad Y = I^C_4 - I^C_2. \tag{24}$$

The sizes of the two LUTs above are determined by the number of bits per pixel of the camera sensor and the number of the projected fringe patterns.

In our proposed method we find it is not convenient to directly solve Eq. (14) because of the amount of time needed to compute $\cos(\bullet)$. As a result, another LUT for $\cos(\bullet)$, namely for K''_n, needs to be created. This may bring in some errors which affect our algorithm described in Sec. 2.2, but as long as more decimal places (five or six) are retained for the calculated radian value, the introduced errors will be so small that they can be ignored. Furthermore, even if some 'bad' pixels have survived from this algorithm because of the tiny errors, they would be detected by our following algorithms. Suppose we retain i decimal places for the radian ω. The LUT for K''_n can be written as below:

$$\mathrm{LUT}K''_n(\omega \cdot 10^i) = \cos(\omega), \tag{25}$$

where $\omega = \Phi(x,y) + 2\pi n/N$, and $\Phi(x,y) \in [-\pi, \pi]$. Thus, the maximum size of this LUT is $4\pi \cdot 10^i$. Relying on the LUT-based method, the "heavy" and time-consuming computation work is preaccomplished, and phase value, intensity modulation, and K''_n can be obtained by a much simpler array indexing operation which greatly reduce the computational cost.

3 Framework

The framework is composed of the following procedures:

1. Calculate phase value and modulations by using a phase-shifting algorithm and two-frequency phase-unwrapping algorithm.
2. By utilizing results from step (1), calculate K'_n and K''_n for each pixel. Then, compute root mean square error. Find a proper threshold to tell invalid pixels apart from valid ones.
3. Compare two modulations of each pixel; the pixels with large modulation variation are invalid pixels.
4. According to modified phase monotonicity criterion, eliminate incorrect pixels with unreliable unwrapped phase.

5. Compare smoothed final phase map with origin final phase map to identify undesirable pixels.

4 Experiments

As shown in Fig. 4, the real-time 3-D measurement system we developed includes a modified DLP commercial projector (ACER X1161PA) having the resolution of 800×600 pixels, a high speed industrial CCD camera GE680 (Allied Vision Technologies) with the resolution of 640×480 pixels, a maximum rate of 205 frames per second (fps), and a self-developed field-programmable gate array (FPGA) board. Since the color wheel of the projector we used spins at 120 Hz, we removed it and sent trigger signal to a DMD chip by our self-developed FPGA board to make it work in monochrome mode at 120 Hz; besides, fringe patterns were rapidly generated and sent to the projector by our FPGA board. And with its help, it was not difficult to accomplish the synchronization between the CCD camera and projector. Consequently, the CCD camera operates at 120 fps. As for our data processing device, we used a Dell OptiPlex 990 with an Intel Core i7 2600, running at 3.4 GHz. To achieve simultaneous data acquisition and processing, four threads separately created for acquisition, 3-D reconstruction, invalid pixels detection, and display were controlled by four CPU cores to realize high-speed, real-time 3-D shape reconstruction. Table 1 shows the constraints concerned with our experiments in which the Gaussian filter is of size 3×3 pixels with standard deviation of 0.5.

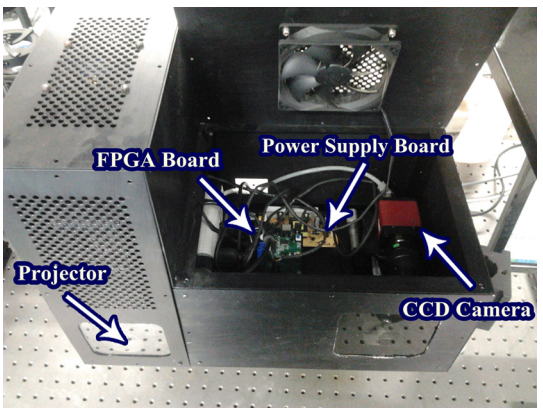

Fig. 4 Our real-time 3-D measurement system (CCD: charge-coupled device; FPGA: field-programmable gate array).

Table 1 Constraints in experiments.

Constraint	Error	σ	Δ_1	Δ_2	V
Value	0.234	0.25	$-\pi/128$	$\pi/8$	0.146

4.1 *Moving Hand*

The measured object was a hand moving up and down at the speed about 0.6 m/s. In this case, a four-step phase-shifting method and two-frequency phase-unwrapping algorithm were adopted. For the two-frequency method, the wavelength of low frequency was the width of the projected pattern. The other wavelength was 1/20th of the previous one. The eight captured images are demonstrated in Fig. 5. Between each high frequency images and low frequency images, there exists a 90-deg. phase shift. Before any steps are performed, to get rid of the effect of shades and background, those pixels with low modulation should be removed in advance. A rough 3-D reconstruction is shown in Fig. 6(a). There were lots of invalid pixels with incorrect phase values present at the contour of the moving hand. To demonstrate the effectiveness of the proposed method, we showed the invalid pixel eliminated results after each step in Fig. 6(b)–6(e). It is plain to see that after performing all the steps of our algorithm, the invalid pixels have been eliminated completely.

In order to better illustrate the proposed method, we carefully examined the whole process, step by step.

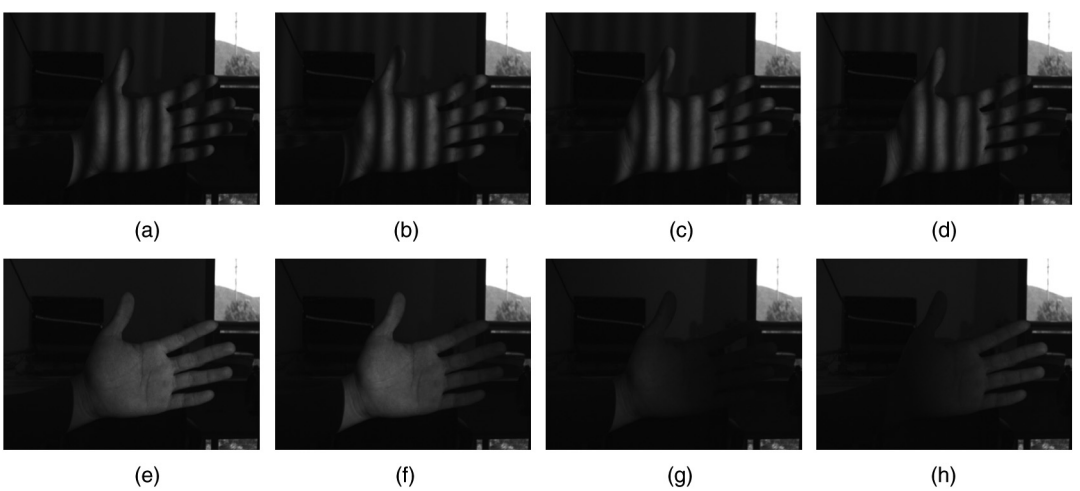

Fig. 5 Captured phase shift images of two frequencies fringe patterns for 3-D measurement of a moving hand: (a) high frequency fringe image (90 deg.); (b) high frequency fringe image (180 deg.); (c) high frequency fringe image (270 deg.); (d) high frequency fringe image (360 deg.); (e) low frequency fringe image (90 deg.); (f) low frequency fringe image (180 deg.); (g) low frequency fringe image (270 deg.); (h) low frequency fringe image (360 deg.).

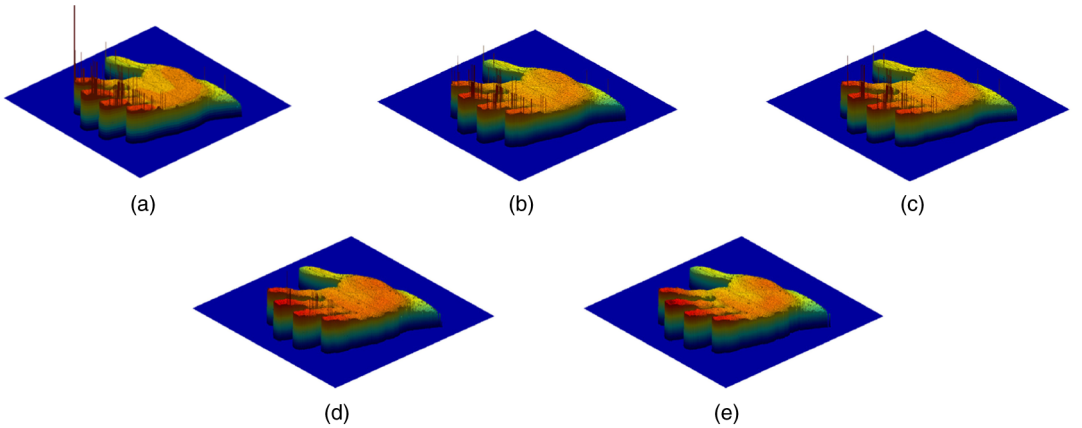

Fig. 6 3-D reconstruction result of a moving hand: (a) 3-D result without invalid pixels identification; (b) 3-D result after the first step; (c) 3-D result after the second step; (d) 3-D result after the third step; (e) accurate 3-D result after all the steps.

1. First step: by employing four-step phase-shifting and two- frequency phase-unwrapping techniques, phase values from two frequencies images were acquired. For high frequency, we put its phase value into the form of $\cos(\bullet)$, namely the $K_n''(n = 1, 2, 3, 4)$. One K_n'' value is shown in Fig. 7(a). By solving Eq. (13), we had $K_n'(n = 1, 2, 3, 4)$, at the same shifted phase, the corresponding map is shown in Fig. 7(b). After computing the root mean square error and comparing it with the *Error*, invalid pixels were detected, and are shown in Fig. 7(c). Similarly, for low frequency, the same procedures could be adopted. One pair of K_n' and K_n'' values is shown in Fig. 7(d) and 7(e), respectively. Although, this result was not as notable as the one obtained from high frequency, it actually detected a few invalid pixels surviving from the prior process, as shown in Fig. 7(f). After the first step, a 3-D result is shown in Fig. 6(b). Obviously, the invalid pixel with the largest final phase value and some unreliable pixels around index finger and middle finger were removed.
2. Second step: to detect phase invalid pixels by comparing two intensity modulations of each pixel. These two modulation maps are shown in Fig. 8. Figure 8(a) shows the modulation map derived from high frequency, and Fig. 8(b) shows the modulation map from low frequency. By using Eq. (16) and the constraint σ, the 'bad' pixels were identified, as shown in Fig. 8(c). After two steps, Fig. 6(c) shows the 3-D result.
3. Third step: comparing the phase of a point and that of its neighborhoods. Those pixels which did not satisfy phase monotonicity, namely Eq. (18), were the points required to be eliminated. The detected pixels are shown in Fig. 8(d). After three refinement steps, the 3-D result is shown in Fig. 6(d).
4. Fourth step: utilizing a Gaussian filter to locate invalid points. The final phase map was smoothed by the Gaussian filter, and with the constraint V, the detected invalid points in this step are shown in Fig. 8(e), and the 3-D result is shown in Fig. 6(e), which is the result

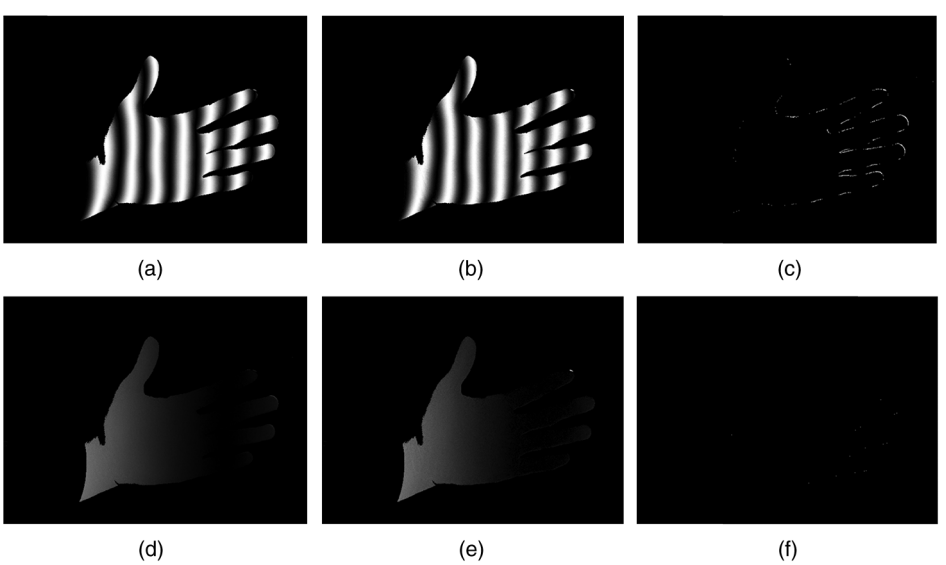

Fig. 7 Comparison between K_n' and K_n'' from each frequency pattern: (a) K_n'' from high frequency pattern at phase shift 90 deg; (b) corresponding K_n' from high frequency pattern at phase shift 90 deg; (c) detected invalid pixels in high frequency pattern; (d) K_n'' from low frequency pattern at phase shift 90 deg; (e) corresponding K_n' from low frequency pattern at phase shift 90 deg; (f) detected invalid pixels in low frequency pattern.

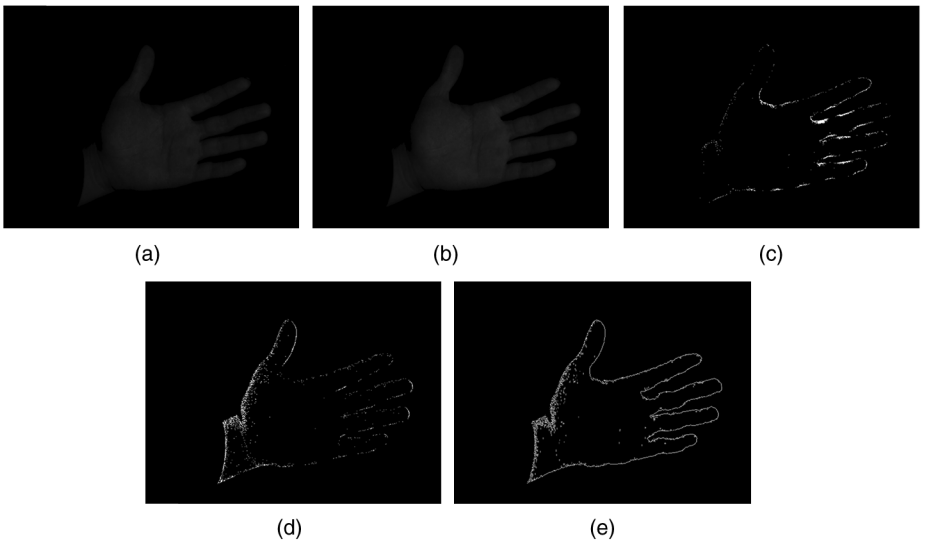

Fig. 8 (a) Modulation map derived from high frequency pattern; (b) modulation map derived from low frequency pattern; (c) invalid pixels detected by comparing the two modulation maps; (d) invalid pixels eliminated by phase monotonicity method; (e) invalid pixels removed by using a Gaussian filter.

Table 2 Experimental time cost.

Processing	Time cost (ms)
Wrapped phase + intensity modulation	1.84
Unwrapped phase	1.45
First step	2.86
Second step	1.43
Third step	1.28
Fourth step	2.47
3D model	2.12
Total	13.45

of accuracy and reliability. Further, the experimental time, averaged over 1000 frames, is listed in Table 2, from which we can see that as the LUT-based algorithm was applied to retrieve the phase value, modulation, and K_n'' values, the 3-D reconstruction time consumption was low. It shows that for each reconstruction, our four-step outlier elimination cost 8.04 ms, and the total time cost of each reconstruction was 13.45 ms (74.35 fps), which is adequate to meet the requirements in real-time measurement.

4.2 *Rotating Dixie Cup*

In order to verify our approach can be used in different situations, in this experiment, a dixie cup rotating at angular speed about 2 rad/s was employed. With words and patterns printed on its surface, invalid pixels would be found at the edge of those words when the cup was rotating because of abrupt variations of the reflectivity. Moreover, those unreliable pixels would also exist at the border of the dixie cup. Two images of four phase-shifting method are shown in Fig. 9(a) and 9(b). The 3-D reconstruction without invalid pixels elimination procedures is shown in Fig. 9(c), and the accurate reconstruction is shown in Fig. 9(d). From the result before invalid points elimination, some outliers can be clearly recognized, while after applying our method, these errors were completely eliminated, resulting in a precise and reliable reconstruction.

5 Conclusion

A novel four-step approach of invalid pixel elimination in high-speed, real-time 3-D shape measurement is presented in this paper. First, by utilizing a phase-shifting algorithm, a phase value is solved. Then, with the purpose of judging its correctness, another phase value at the same pixel is obtained by taking advantage of the captured intensity, modulation, and average intensity at that pixel. If the two phase values are close enough, the tested pixel is a valid one. Otherwise, it is a "bad" one. To lower the computational complexity, we retained both phase values in their forms of cos(•), and create a LUT for cos(•). By calculating root mean square error, the invalid pixel will have a much bigger error than the valid pixel. Second, we compare two modulations derived from two wavelength patterns because of the invariableness of the reflectivity. Third, we compare the neighboring pixel's phase value by the monotonicity of unwrapped phase toward a specific direction. And the last step is to compare the final phase map with itself, which has been smoothed by a Gaussian filter. After the four steps mentioned above, invalid points, such as the points around the edge of the moving object or scattered border of two different materials, are detected and eliminated. Ascribed to LUT-based fast data processing algorithm, our proposed method can be done in 8.04 ms, and the overall process for 3-D reconstruction can be realized at 74.35 fps. The results of experiments have verified the practical applicability of the proposed approach.

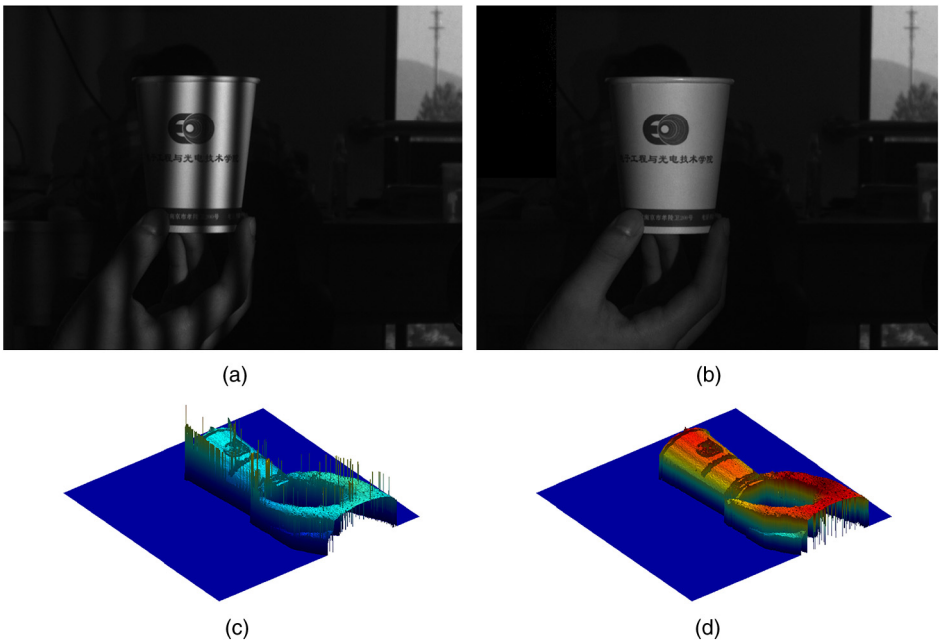

Fig. 9 Real-time measurement of a rotating dixie cup: (a) high frequency fringe image (90 deg); (b) low frequency fringe image (90 deg); (c) 3-D reconstruction result of a rotating dixie cup before invalid pixels elimination; (d) 3-D result of a rotating dixie cup after four-step invalid pixels elimination.

Some weaknesses of this approach have to be mentioned. One is that the proposed invalid point-eliminating method is based on a phase-shifting algorithm, and the total number of phase shifts (N) should be greater than three. In several tests with a three-step phase-shifting algorithm, results showed that for either "good" pixels or "bad" pixels, the respective K_n' and K_n'' values are identical, so the first step of the proposed approach will not work. The other concern is our presented algorithms are based on an assumption that the speeds of projection and capture can keep up with the movement of the measured object. Otherwise, the phase may not be correctly recovered. If the object moves faster, as long as the rates of projection and capture also increase to that extent, it is not difficult to accurately retrieve its phase and to apply our work to detect its outliers.

Acknowledgments

This project was supported by the Research Fund for the Doctoral Program of Ministry of Education of China (No. 20123219110016) and the Research and Innovation Plan for Graduate Students of Jiangsu Higher Education Institutions, China (No. CXZZ11_0237).

References

1. F. Chen, G. M. Brown, and M. M. Song, "Overview of three-dimensional shape measurement using optical methods," *Opt. Eng.* **39**(1), 10–22 (2000).
2. S. S. Gorthi and P. Rastogi, "Fringe projection techniques: Whither we are?," *Opt. Laser Eng.* **48**(2), 133–140 (2010).
3. S. Zhang, "Recent progresses on real-time 3D shape measurement using digital fringe projection techniques," *Opt. Laser Eng.* **48**(2), 149–158 (2010).
4. T. Weise, B. Leibe, and L. Van Gool, "Fast 3D scanning with automatic motion compensation," in *IEEE Conf. on Comput. Vis. and Pattern Recognit.*, pp. 1–8, IEEE, Minneapolis, Minnesota (2007).
5. D. L. Lau, K. Liu, and L. G. Hassebrook, "Real-time three-dimensional shape measurement of moving objects without edge errors by time-synchronized structured illumination," *Opt. Lett.* **35**(14), 2487–2489 (2010).
6. Y. J. Wang, S. Zhang, and J. H. Oliver, "3D shape measurement technique for multiple rapidly moving objects," *Opt. Express* **19**(9), 8539–8545 (2011).
7. J. Li et al., "Optimized two-frequency phase-measuring-profilometry light-sensor temporal-noise sensitivity," *J. Opt. Soc. Am. A* **20**(1), 106–115 (2003).
8. Y. C. Wang et al., "Maximum SNR pattern strategy for phase shifting methods in structured light illumination," *J. Opt. Soc. Am. A* **27**(9), 1962–1971 (2010).
9. K. Liu et al., "Dual-frequency pattern scheme for high-speed 3-D shape measurement," *Opt. Express* **18**(5), 5229–5244 (2010).
10. S. Zhang and P. S. Huang, "High-resolution, real-time three-dimensional shape measurement," *Opt. Eng.* **45**(12), 123601 (2006).
11. C. Zuo et al., "High-speed three-dimensional profilometry for multiply objects with complex shapes," *Opt. Express* **20**(17), 19493–19510 (2012).
12. S. Zhang, "Phase unwrapping error reduction framework for a multiple-wavelength phase-shifting algorithm," *Opt. Eng.* **48**(10), 105601 (2009).
13. F. Chen, X. Su, and L. Xiang, "Analysis and identification of phase error in phase measuring profilometry," *Opt. Express* **18**(11), 11300–11307 (2010).
14. L. Huang and A. Anand Krishna, "Phase invalidity identification framework with the temporal phase unwrapping method," *Meas. Sci. Technol.* **22**(3), 35304–35308 (2011).
15. C. Zuo et al., "Optimized pulse width modulation pattern strategy for three-dimensional profilometry with projector defocusing," *Appl. Opt.* **51**(19), 4477–4490 (2012).

Biographies and photographs of the authors are not available.